Incorporative mixing in microreactors: Influence on reactions and importance of inlet designation

Asano, Shusaku

Maki, Taisuke

Inoue, Shogo

Sogo, Sumito

他

出版情報：Chemical Engineering Journal. 451, pp.138942-, 2023-01. Elsevier
バージョン：
権利関係：Creative Commons Attribution 4.0 International

Chemical Engineering Journal 451 (2023) 138942

Contents lists available at ScienceDirect

Chemical Engineering Journal

journal homepage: www.elsevier.com/locate/cej

Incorporative mixing in microreactors: Influence on reactions and importance of inlet designation

Shusaku Asano [a,*], Taisuke Maki [b], Shogo Inoue [b], Sumito Sogo [b], Masashi Furuta [b], Satoshi Watanabe [b], Yosuke Muranaka [b], Shinji Kudo [a], Jun-ichiro Hayashi [a], Kazuhiro Mae [b]

[a] Institute for Materials Chemistry and Engineering, Kyushu University, Kasuga 816-8580, Japan
[b] Department of Chemical Engineering, Graduate School of Engineering, Kyoto University, Japan

ARTICLE INFO

Keywords:
Microreactor
Mixing
Villermaux-Dushman reaction
Computational fluid dynamics
Particle synthesis
3D printing

ABSTRACT

Fast mixing is an essential feature of a microreactor. This study reveals the critical role of microscopic fluid incorporation on fast chemical reactions in a microreactor. The vortices in a microreactor produce tiny fluid segments, and the incorporation of these segments into the surrounding fluid triggers chemical reactions. The selectivity of chemical reactions highly depends on the type of the fluid segment incorporated into the fluid. Microreactor operations that consider incorporative mixing can achieve better reaction results, even with slow mixing. For example, a tee mixer showed better reaction performance with the vertical confluence configuration than with the symmetric configuration, although the symmetric 180-degree confluence provides more intense mixing. Computational fluid dynamics (CFD) simulations showed that vertical confluence enabled the division and incorporation of a stream from the horizontal inlet into another stream. The appropriate inlet designation is vital when two inlets of a microreactor differ in dimensions, directions, or positions because the different inlets provide different mixing profiles. The two inlets of the microreactor were distinguishable even though the fabrication error was insignificant. For instance, feed orientations changed the side-product yield seven times in a 3D-printed microreactor. Moreover, the impact of incorporative mixing on particle synthesis was confirmed. Switching the two inlets significantly influenced the morphology and size of the synthesized particles by changing the initial nucleation environment. In conclusion, considering incorporative mixing and optimal inlet orientation will enhance the performance and flexibility of microreaction technology.

1. Introduction

Microreactors with small internal structures have been studied and applied in several fields of organic chemistry and material synthesis [1–3]. Fast mixing is an essential feature of microreactors [4,5]. Efficient synthetic pathways for fine chemicals [6,7], protecting-group-free halogen-lithium exchange reactions [8,9], and size-controlled nanoparticle synthesis [10–15] have been achieved using microreactors. A smaller reactor has a better mixing performance but causes a larger pressure loss and has higher clogging risks. Therefore, the design and optimization of microreactors is crucial for industrial applications [1,16]. An operation with a higher Reynolds number ($>10^2$) is the standard for fast mixing with increased throughput in industrial applications.

Competing chemical test reactions are common techniques used to evaluate the physical mixing quality in microreactors [17–19]. In chemical test reactions, an instantaneous main reaction is coupled with a relatively slow side reaction such that better mixing produces fewer side products. Examples of test reactions include the diazo coupling between 1-naphthol and diazotized sulfanilic acid [20], bromination of 1,3,5-trimethoxybenzene [21], and Villermaux-Dushman reaction. The Villermaux-Dushman reaction has been the most commonly used test reaction owing to its safety, ease of measurement, and adjustable sensitivity. Another method for mixing characterization has been proposed [22] but has not replaced the Villermaux-Dushman reaction yet [23,24]. The Villermaux-Dushman reaction couples the neutralization and comproportionation of iodide and iodate ions to form iodine [25]. The formation of triiodide enables the easy quantification of the side product using UV–Visible spectroscopy. The schemes are as follows:

$H_2BO_3^- + H^+ \rightleftarrows H_3BO_3$ (main reaction).

* Corresponding author.
E-mail address: shusaku_asano@cm.kyushu-u.ac.jp (S. Asano).

https://doi.org/10.1016/j.cej.2022.138942
Received 14 June 2022; Received in revised form 7 August 2022; Accepted 28 August 2022
Available online 1 September 2022

$5I^- + IO_3^- + 6H^+ \rightleftarrows 3I_2 + 3H_2O$ (side reaction).

$I_2 + I^- \rightleftarrows I_3^-$ (equilibrium).

For a mixing evaluation using the Villermaux-Dushmn reaction, an acid solution and basic buffer solution containing iodide and iodate ions are mixed. If the mixing is fast enough, all protons in the acid solution react with the base because neutralization has extremely fast kinetics. However, if the mixing proceeds slowly, several protons react with iodide and iodate ions to form iodine because mass transfer limits the neutralization rate. Most previous studies have assumed that the mixing time in microreactors solely determines the side product yield [26–28]. With this assumption, the optimal structure and operating conditions have been discussed in terms of the trade-off between the pressure loss requirement and the mixing time [17,18].

However, Kölbl and Kraut demonstrated that another factor influences the reaction when the mixing time was maintained constant using an asymmetric tee mixer (Fig. 1(a)) [29]. When the acid solution was fed from a narrower inlet, the iodine yield decreased by 15–35 % compared to another orientation in which the acid solution was supplied from a wider inlet. In both orientations, the solutions had the same flow rate; therefore, the mixing times were constant. Our previous study evaluated the microjet mixers illustrated in Fig. 1(b) and observed that the feed orientation influenced the test reaction results [30]. The Villermaux-Dushman reaction and bromination of 1,3,5-trimethoxybenzene were conducted. Feeding an acid solution from the inner inlet resulted in a much smaller iodine yield in the Villermaux-Dushman reaction. For the bromination reaction, providing the bromine solution from the inner inlet suppressed the side product formation to less than one-tenth of the other orientation. These previous studies indicate that a more detailed understanding of the mixing profile is necessary for the design and operation of microreactors.

This study was conducted based on the assumption that a model considering the incorporation of one fluid into another fluid generally explains the above examples. Fig. 2 illustrates the concept of incorporative mixing focused in this study. Fig. 2(a) shows the typical mixing profile of fluids A and B in a microreactor reproduced by a computational fluid dynamics (CFD) simulation. The confluence of fluids produces vortices of various scales, from the reactor diameter length to the Kolmogorov scale. Smaller vortices disappear faster owing to diffusion into the surrounding fluid. Fig. 2(b) illustrates fluid division and incorporation in a simplified scheme. The vortices divide and rearrange the fluid. In some regions, small fluid segments are present inside the other fluid. They are rapidly incorporated into their surroundings. The remaining larger pieces then merge by exchanging components with each other. The convective fluid division followed by the incorporation into another fluid is termed as an incorporative mixing in the present study. The incorporation of fluid during the mixing was studied decades ago as a tool for simplifying the mixing process [31,32]. However, these studies focused on the mathematical treatment of the mixing and the estimation of a mixing time. In the present study the influence of the incorporative mixing on the reaction selectivity is considered in depth.

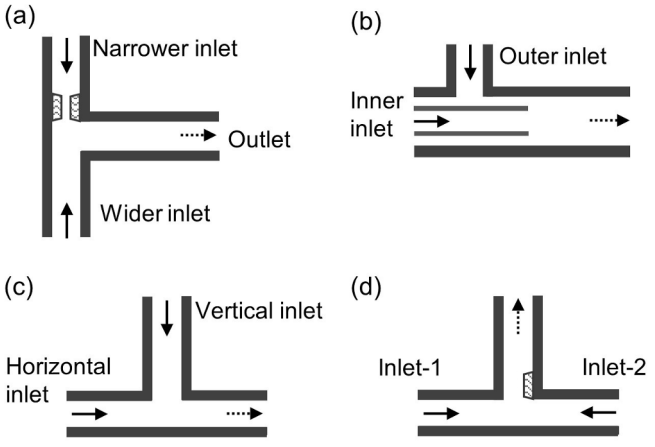

Fig. 1. Examples of microreactors with distinguishable inlet ports: (a) tee mixer with one narrowed inlet, (b) microjet mixer with concentric structure, (c) tee mixer with vertical confluence orientation, and (d) symmetric mixer with a fabrication error.

When the two inlets of a microreactor are identical, as shown in Fig. 2(a), the portion of both fluids (A and B) incorporated into each other is the same. However, when a microreactor has unique inlets (Fig. 1), these portions can be specific to each inlet (Fig. 2(c)). Therefore, inlet orientation can change the reaction selectivity. In the Villermaux-Dushman reaction, side products produced after incorporating the acid solution into the buffer solution were negligible. In contrast, combining the buffer solution with the acid solution resulted in side reactions by iodide and iodate in an acidic environment. This scheme explains the previous reports on asymmetric tee and microjet mixers. Fluids fed from the narrower inlet and the inner inlet undergo incorporative mixing with the other fluid in a significant portion.

This study aimed to validate the generality and importance of the concept of incorporative mixing and its influence on chemical reactions. First, we explored the influence of inlet orientation on chemical reactions in practical situations. As an example, a vertically configured tee mixer was investigated (Fig. 2(c)). Owing to space limitations, vertical confluence often appears in microchips [33,34] and in sequential mixing processes [35,36]. A 3D-printed microreactor was also examined as an example of a structure with a fabrication error (Fig. 1(d)). Moreover, various particle syntheses in a microjet mixer were investigated to determine the possibility of controlling the particle morphology and size by designing detailed mixing profiles. Traditional particle synthesis often employs the dropwise addition of one solution to the stirred solution. Addition methods (A-to-B or B-to-A) are considerably more influential than the stirring and dropping rates [37–39]. It was expected that incorporating mixing in a microreactor would play a significant role in particle formation, similar to the addition methods used in traditional procedures.

2. Methodology

2.1. Materials

Potassium iodide, potassium iodate, boric acid, chloroplatinic acid hexahydrate, sodium tetrahydroborate, polyvinylpyrrolidone (PVP, M. W. 1,300,000), 5 M hydrochloric acid solution, 5 M sodium hydroxide solution, ethanol, copper (II) trifluoromethanesulfonate, and 4,4′-bipyridine were purchased and used without further purification. Ultrapurified water was prepared using a Milli-Q water purification system and was used throughout the experiment.

2.2. Microreactors

The microreactors consisted of micromixers and tubes. Outlet tubes with a length of 0.30 m and an inner diameter of 0.5 mm were connected to the micromixers. These outlet tubes were placed straight to minimize external disturbances during the mixing process.

2.2.1. Tee mixer

A tee mixer with an internal diameter of 0.33 mm (Swagelok, Solon, USA) was used. A tee mixer was configured symmetrically with 180-degree confluence or asymmetrically with 90-degree confluence, as shown in Fig. 1(c).

2.2.2. KM-SUS mixer

A KM mixer features instant and uniform mixing enabled by the central collision of substreams [40]. The original KM mixer (KM-SUS, Fig. 3(a)) was mechanically fabricated using stainless-steel plates. Substreams of dimensions 0.1 mm (width) × 0.1 mm (height) were etched

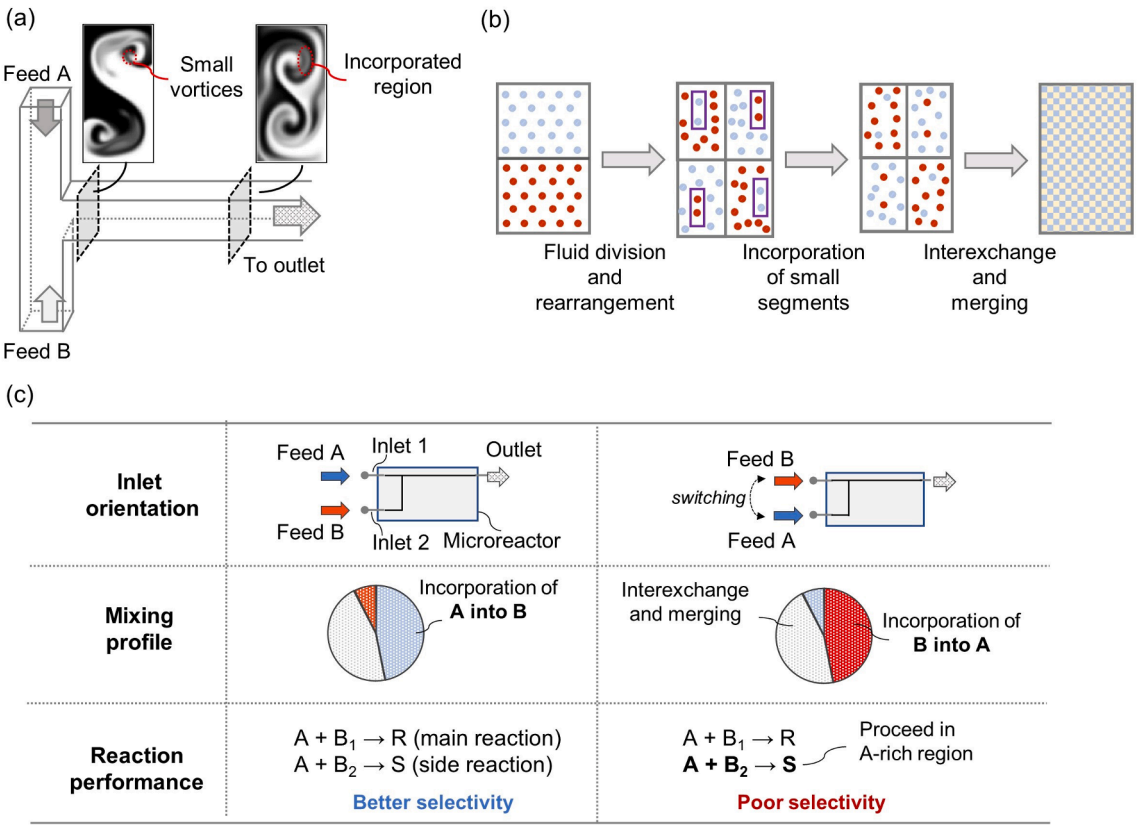

Fig. 2. Concept of the incorporative mixing: (a) typical mixing profile in a microreactor reproduced in the CFD simulation showing the small fluid segments incorporated into the surrounding fluid, (b) simplified illustration of the mixing process in a microreactor, and (c) influence of inlet orientation on the mixing profile. CFD simulation was performed for mixing water in a tee with 0.1 × 0.1 mm inlet channels and a 0.1 × 0.2 mm outlet channel. Total flow rate was 2.4 mL/min.

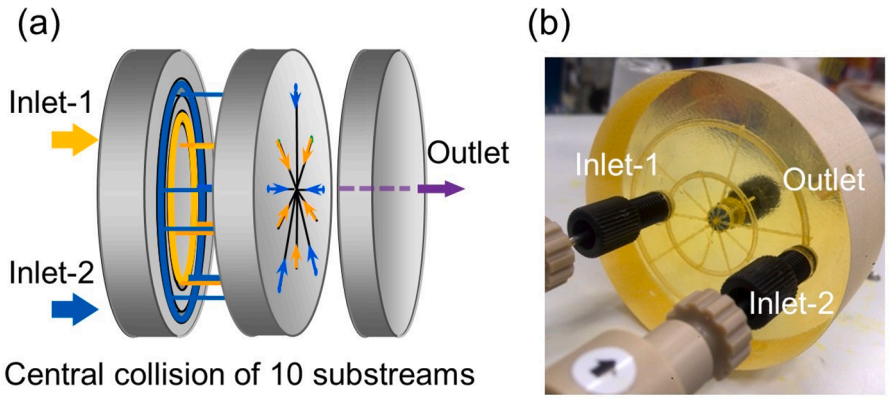

Fig. 3. KM mixer with 5 × 2 substreams: (a) Schematics of the original product consisting of mechanically fabricated stainless-steel plates (KM-SUS), and (b) photograph of the imitation product printed with an acrylate resin (KM-3Dprint).

on the second plate. The center of the substreams had a diameter of 0.32 mm. The outlet hole had a diameter of 0.36 mm and length of 1 mm. The two inlets were named inlet-1 and inlet-2, but these inlets were identical in terms of the mixing profile. The internal structure around the mixing point is shown in Figure S1 as a computer aided design drawing.

2.2.3. KM-3Dprint mixer

The imitation KM mixer (KM-3Dprint, Fig. 3(b)) was directly printed from a computer design using an inkjet 3D printer (Agilista, Keyence, Osaka, Japan) and UV-curable acrylate polymer (Keyence). The printer had a resolution of 40, 64, and 15 μm in the *x*-, *y*-, and *z*-directions, respectively. The measured errors were 150 μm in the *x*-, *y*-directions and 20 μm in the *z*-direction at the maximum [41]. Due to the much larger errors of the 3D printing than the mechanical fabrication used for the KM-SUS, the dimensions of the substreams of KM-3Dprint were designed to be 0.5 mm width × 0.2 mm height. The diameter of the center hole was set to be 1.5 mm.

2.2.4. Microjet mixer

Based on a previous report [30], three microjet mixers were assembled using commercial tees and tubes as in Fig. 1(b). Table 1 lists the dimensions. The outer tubes of the microjet mixers were extended 0.3 m as the outlet tubes.

Table 1
Dimensions of microjet mixers in mm.

Name	Inner diameter of the inner tube	Outer diameter of the inner tube	Inner diameter of the outer tube
Jet_S	0.10	0.36	0.50
Jet_M	0.18	0.79	1.00
Jet_L	0.50	0.79	2.40

2.3. The Villermaux-Dushman reaction

The Villermaux-Dushman reaction was conducted according to the method described by Commenge and Falk [26]. Hydrochloric acid solution and alkaline buffer solution containing potassium iodide, potassium iodate, and boric acid were mixed at the same flow rate. Aqueous solutions of the acid and buffer were prepared at the following concentrations:

- acid solution: [HCl] = 60 mM
- buffer solution: [KI] = 32 mM, [KIO_3] = 6 mM, [NaOH] = 90 mM, and [H_3BO_3] = 90 mM.

The solutions were fed into the device using 260D syringe pumps (Teledyne Isco, Lincoln, USA) at room temperature of 20 ± 5 °C. The samples were collected from the outlet tubes into optical cells with an observation length of 1 cm. The absorbance (ABS) at 353 nm specific to triiodide ions was measured after the sample collection phase using a UV-Mini 1240 spectrometer (Shimadzu, Kyoto, Japan). The error bars in the figures for the Villermaux-Dushman reaction results indicate the standard deviation of at least three analyses.

2.4. $CaCO_3$ precipitation

$CaCO_3$ was precipitated by mixing 50 mM aqueous solutions of $CaCl_2$ and Na_2CO_3 at the same flow rate at room temperature of 20 ± 5 °C. The outlet suspension was filtered through a 0.1 μm pore membrane filter (Advantec, Tokyo, Japan) and dried at 60 ℃ under vacuum. Powder samples were identified using powder X-ray diffraction (XRD, Multiflex, Rigaku, Tokyo, Japan) patterns at room temperature and were observed using scanning electron microscopy (SEM, JSM-6700F, Jeol, Tokyo, Japan). Precipitation of $CaCO_3$ in a batch reactor was conducted for comparison. 10 mL of 50 mM aqueous solution of Na_2CO_3 (or $CaCl_2$) solution was stirred at 1000 rpm in a beaker. The same amount of 50 mM aqueous solution of $CaCl_2$ (or Na_2CO_3) was then poured into the beaker. The suspension was kept under stirring for 10 min. Then, the suspension was filtered through a 0.1 μm pore membrane filter and dried at 60 ℃ under vacuum.

2.5. ELM-12 synthesis

An elastic-layered metal–organic framework (MOF)-12, {ELM-12: [$Cu(CF_3SO_3)_2$ (4,4′-bipyridine)$_2$]} [42,43] was synthesized in a microjet mixer by employing a procedure based on a previous report using a vigorously stirred batch reactor [44]. A 30 mM solution of $Cu(OTf)_2$ in water and a 60 mM solution of 4,4′-bipyridine in ethanol were mixed at the same flow rate. Owing to the temperature sensitivity of the MOF synthesis process, mixers and tubes were placed in a water bath at 20.0 ℃. The outlet suspension was maintained at 20.0 ℃ for 15 min and then filtered with a 0.1 μm pore membrane filter and dried at room temperature in a vacuum. Powder XRD patterns were used to identify the powder sample. The powder was observed using SEM, and the edge lengths were measured. The particle size distribution was obtained by measuring the diameter of approximately 200 particles in the SEM images. The error bars on the figure for the ELM-12 synthesis indicate the standard deviation in the edge lengths of the measured particles.

2.6. Pt nanoparticle synthesis

Pt nanoparticles were prepared by mixing an aqueous solution of H_2PtCl_6 and PVP with another aqueous solution of $NaBH_4$ at the same flow rate at room temperature of 20 ± 5 °C. The concentration of H_2PtCl_6 in the stock solution, [Pt^{4+}], was 2 mM. The concentrations of the PVP monomer, [PVP], and $NaBH_4$ in the other stock solution, [$NaBH_4$], were 20 and 8 mM, respectively, under standard conditions. After mixing, one drop of the suspension was placed onto a carbon-coated copper grid (NP-C15, Okenshoji, Japan) and dried at 60 ℃ under vacuum. The particles were observed using transmission electron microscope (TEM, JEM-1010, JEOL, Japan) at 100 kV. The particle size distribution was obtained by measuring the diameter of approximately 200 particles in the TEM images. The error bars on the figures illustrating the Pt nanoparticle diameter indicate the standard deviation of the measured diameter.

2.7. CFD simulation

The commercial finite-volume code FLUENT (version 14.5 and 2021 R2) was employed for the CFD simulation. We simulated the mixing of fluids A and B in tee and KM mixers. Both fluids have the same physical properties and flow rates. The density and viscosity of the fluids were 1000 kg m^{-3} and 0.001 Pa s, respectively. The diffusivity of all the species was 10^{-9} m^2 s^{-1} as the usual value for small molecules in a liquid at ambient temperatures [45]. A 3D laminar flow model was employed. The simulations were performed in a steady state.

The channel shape was modified to minimize numerical diffusion [46] by avoiding circular shapes. The tee mixer was recomposed of square channels with a 0.33 mm edge length. The outlet channel of the KM mixer was a regular decahedron channel with a 0.10 mm edge length. The outlet channel length was 35 mm for both the mixers.

Mixing without chemical reactions was simulated in a KM mixer and a symmetrically configured tee mixer. The tracer species were added to each inlet stream, and their properties were identical to those of the solvent. Mixing with the following parallel-competing reaction system was simulated in a tee mixer.

$A + B_1 \rightarrow R$, $r_1 = k_1[A][B_1]$,.$k_1 = 50000\ M^{-1}s^{-1}$

$A + B_2 \rightarrow S$, $r_2 = k_2[A][B_2]$,.$k_2 = 1000\ M^{-1}s^{-1}$

k_1 was set to simulate a very fast reaction which takes place in the mixing zone [47]. k_2 was set to simulate a side reaction which proceeds with poor mixing [21,48]. Fluid A contained species A at a concentration of 1.0 M. Fluid B contained species B_1 and B_2 at each concentration of 1.0 M. The selectivity of the side product S_S was defined as follows and calculated at the outlet cross section:

$$S_S = \text{molar flow rate of S}/(\text{molar flow rate of R} + \text{molar flow rate of S})$$

The mixing quality α_m at each cross section was defined as the standardized variance of the concentration field [49]:

$$\alpha_m = 1 - \sqrt{\frac{\sigma_c^2}{\sigma_{c0}^2}}$$

$\sqrt{\sigma_c^2}$ is the standard deviation of the mass fraction of the tracer species. $\sqrt{\sigma_{c_0}^2}$ is the initial standard deviation calculated from inlet concentrations and flow rate.

The iterations were conducted at least 2500 times. The residual was smaller than 10^{-4} within 400 iterations. Mesh size dependency was tested by repeating the mesh refinement. Figure S2 shows the test results.

3. Results and discussion

3.1. Significance of incorporative mixing and inlet orientation

Fig. 4(a) shows the results of the Villermaux-Dushman reaction conducted using the tee mixer. The tee mixer with the vertical-confluence configuration showed a high dependency on the inlet orientation, especially at a low total flow rate. When the acid solution was fed from the horizontal inlet and the base solution from the vertical inlet (vertical-1), the ABS values corresponding to the side product yield were less than half of those obtained with the opposite inlet orientation (vertical-2). The tee mixer with the vertical confluence configuration had identical inlet dimensions. Therefore, Fig. 4(a) shows that the two feed streams act differently only with differences in direction. Significantly, both the acid and base solutions used for the Villermaux-Dushman reaction were dilute so that inlet switching did not alter the physical mixing behavior.

Considerably, the side product yield in the vertical-1 configuration was significantly lower than that in the 180-degree confluence configuration (symmetric). Better reaction selectivity of vertical-1 than symmetric is surprising because it is common sense that the 180-degree confluence configuration has higher mixing performance than the 90-degree. Many studies have confirmed more intense vortices and better mixing performance in the 180-degree confluence than in the 90-degree [50–52]. Investigating the optimal inlet orientation might be more important than examining the intensity of the vortices at the mixing point for improving the selectivity of fast chemical reactions.

Fig. 4(b) shows the results obtained using the KM-3Dprint. The flow rate of less than 200 mL/min resulted in the saturation of absorbance. The structure of the KM-3Dprint designed in the computer is identical for the two feed streams. If the fabrication error is negligible, switching the two inlets should not affect the Villermaux-Dushman reaction. The poor fabrication precision should have distinguished the two inlets. Three-dimensional printing (or additive manufacturing) technology has been extensively employed for manufacturing microreactors [53] despite fabrication errors [54]. Therefore, a careful investigation of inlet orientation for 3D-printed microreactors is recommended from the current results.

The CFD simulations were conducted for the tee mixer to discuss the origin of the selectivity difference in detail. The simulations included a simplified parallel competing reaction system. The Villermaux-Dushman reaction was not considered because its kinetics are too complicated [55] for a generalized discussion. In the simulated scheme, B_1 and B_2 compete for the consumption of A. The inherent kinetic constant of $A + B_1 \rightarrow R$ was 50 times higher than that of $A + B_2 \rightarrow S$. Therefore, the role of A was analogous to that of an acid in the Vilermaux-Dushman reaction.

Fig. 5 shows the results of the CFD simulation. Fig. 5(a) shows a mixing profile in the vertical-1 configuration. As shown in the enlarged contour, a portion of the fluid from the horizontal inlet moved to the upper side. The secondary flow, termed the Dean flow [56,57], was responsible for the movement and division of the stream. Consequently, the fluid from the vertical inlet rolled the divided parts into the central part. Both the main reaction and side reaction proceeded at the interface of the streams (Fig. 5(b) and (c)). The vertical-2 configuration showed almost the same profiles in terms of the mixing and the main reaction (Fig. 5(d) and (e)). However, as shown in Fig. 5(f), the B_2 taken into the A-rich region caused a side reaction exclusively. The resulting S_S values

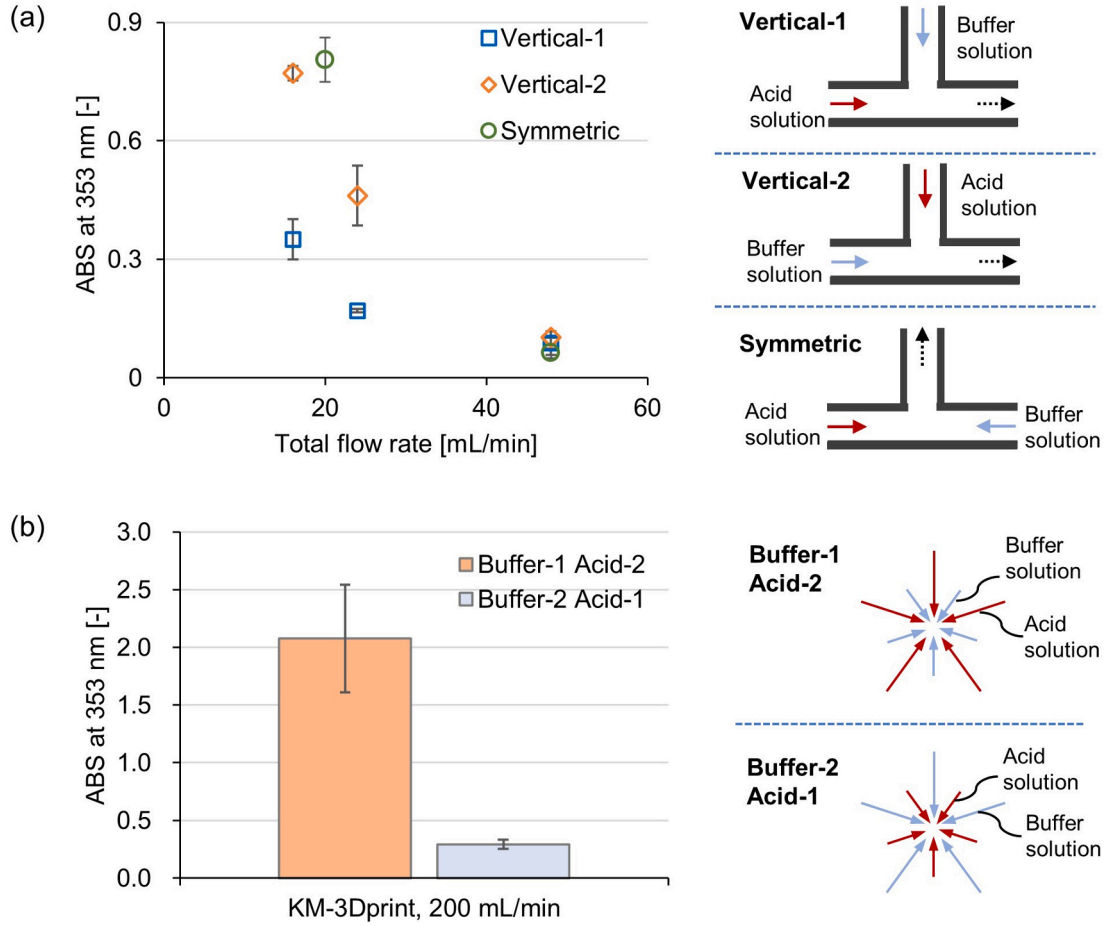

Fig. 4. Results of the Villermaux-Dushman reaction with various inlet configurations: (a) Tee mixer with the vertical confluence configuration and (b) KM-3Dprint.

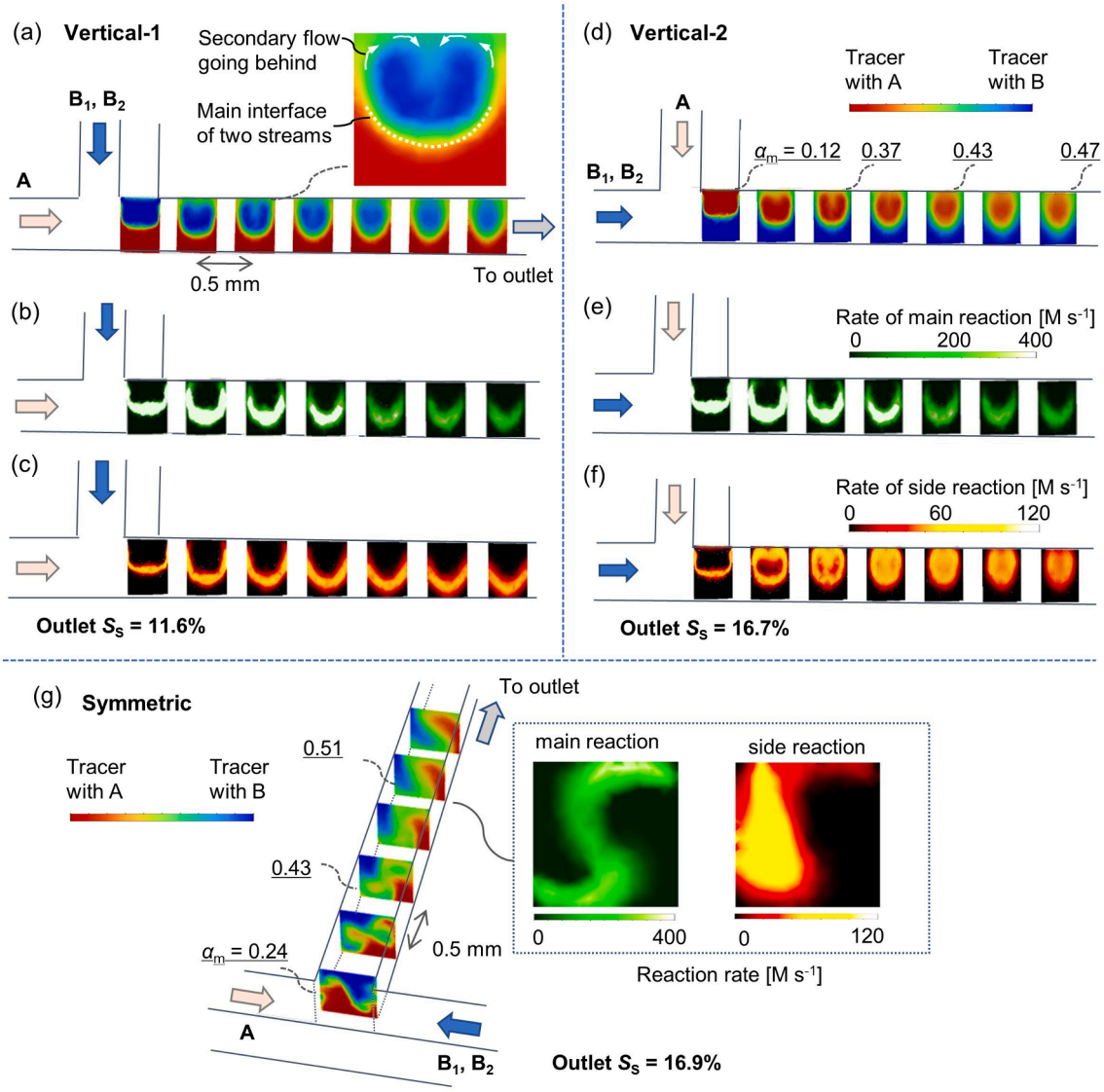

Fig. 5. Profiles of mixing and reaction in the tee mixer with a total flow rate of 13.1 mL/min: (a) tracer concentration, (b) main reaction rate, and (c) side reaction rate in the vertical-1 configuration; (d) tracer concentration with mixing degree α_m, (e) main reaction rate, and (f) side reaction rate profile in the vertical-2 configuration; (g) tracer concentration profile with selected reaction rate contours in the symmetric configuration. α_m in vertical-1 was identical to that in vertical-2.

of 11.6 % and 16.7 % for each orientation were aligned with the experimental results, as shown in Fig. 4(a). The revealed mixing and reaction profiles corroborate the understanding based on the incorporative mixing. Many portions of the stream from the horizontal inlet undergo incorporative mixing with the other stream. Fig. 5(g) shows the mixing and reaction profiles in the symmetric configuration. The mixing was more intense than that at the 90-degree confluence owing to the engulfment flow [58]. The mixing quality α_m at cross sections were higher than that of corresponding positions in the vertical configurations (Fig. 5(d) and (g)). However, the output of S_S was 16.9 %, which is higher than both vertical configurations. The engulfment flow effectively facilitated mixing but allowed the side reaction to proceed in the A-rich region (inset of Fig. 5(g)).

The distinction of inlets was possible even when the two inlet streams were identical in flow rate and dimension, as confirmed through the CFD simulations. The difference in direction resulted in a significant difference in selectivity. A careful assessment of the inlet orientation is vital if a microreactor has different inlets. Consequently, a limitation of the applicable domain of chemical test reactions for mixing evaluation arises. As confirmed by the tee mixer configurations, intensified mixing does not always result in better reaction selectivity. Therefore, comparing test reaction scores derived from reaction selectivity may not be useful for comparing physical mixing behaviors. In the last part of this paper, the possibility of using a new mixing evaluation scheme to accurately assess physical mixing behaviors has been discussed.

3.2. *Influence of incorporative mixing on particle synthesis*

The influence of incorporative mixing on particle synthesis processes was examined. Microjet mixers were used for this purpose because they can clearly distinguish the two feed streams and are resistant to clogging [59].

3.2.1. *$CaCO_3$ precipitation*

Fig. 6 shows SEM images of the $CaCO_3$ particles obtained using the microjet mixer (Jet_S). Switching the inlet orientation significantly changed the particle morphology. When the Na_2CO_3 solution was fed from the inner inlet and the $CaCl_2$ solution from the outer inlet, spherical

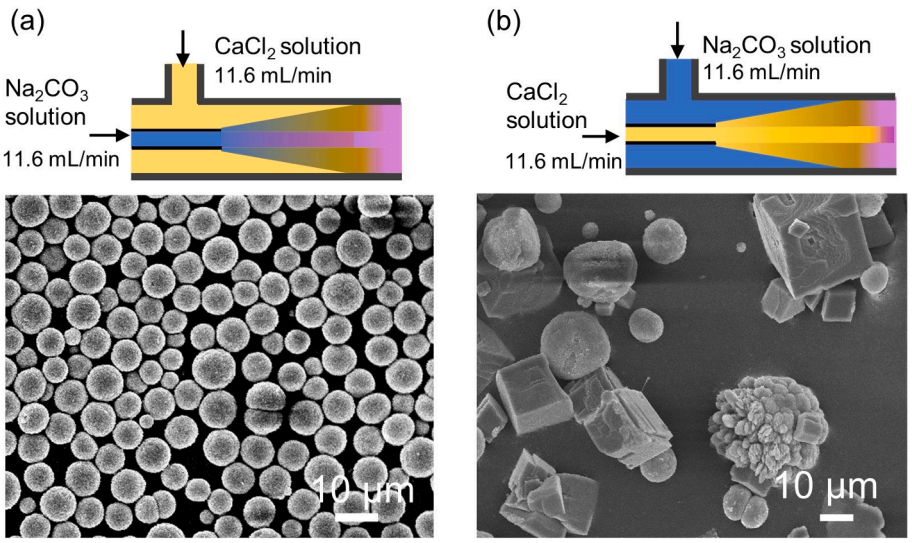

Fig. 6. SEM images of $CaCO_3$ particles synthesized in a microjet mixer (Jet_S) with a total flow rate of 23.2 mL/min: (a) Na_2CO_3 solution was fed from the inner inlet, and (b) $CaCl_2$ solution was fed from the inner inlet.

particles with a diameter of 5–10 μm were obtained. The XRD pattern (Figure S3) confirmed that the crystals were vaterite [60]. The other orientation results in rhombohedral crystals with vaterite agglomerates. The XRD patterns confirmed that they were a mixture of calcite and vaterite. The most plausible explanation is the effect of pH on the crystallization. Kogo et al. investigated the $CaCO_3$ formation process by adjusting the initial pH using HCl and NH_3 [61]. A lower pH favored single-phase vaterite formation, and a higher pH favored calcite formation. Incorporating the Na_2CO_3 solution into the $CaCl_2$ solution is favorable for synthesizing vaterite because of the lower pH of the $CaCl_2$ solution.

To clarify the role of fast mixing in a microreactor, $CaCO_3$ precipitation in a batch reactor was conducted by adding one solution to the other solution stirred in a beaker. Pure calcite particles without vaterite were formed regardless of the addition methods (Na_2CO_3-to-$CaCl_2$ or $CaCl_2$-to-Na_2CO_3) (Figure S4). The thermodynamic stability of these

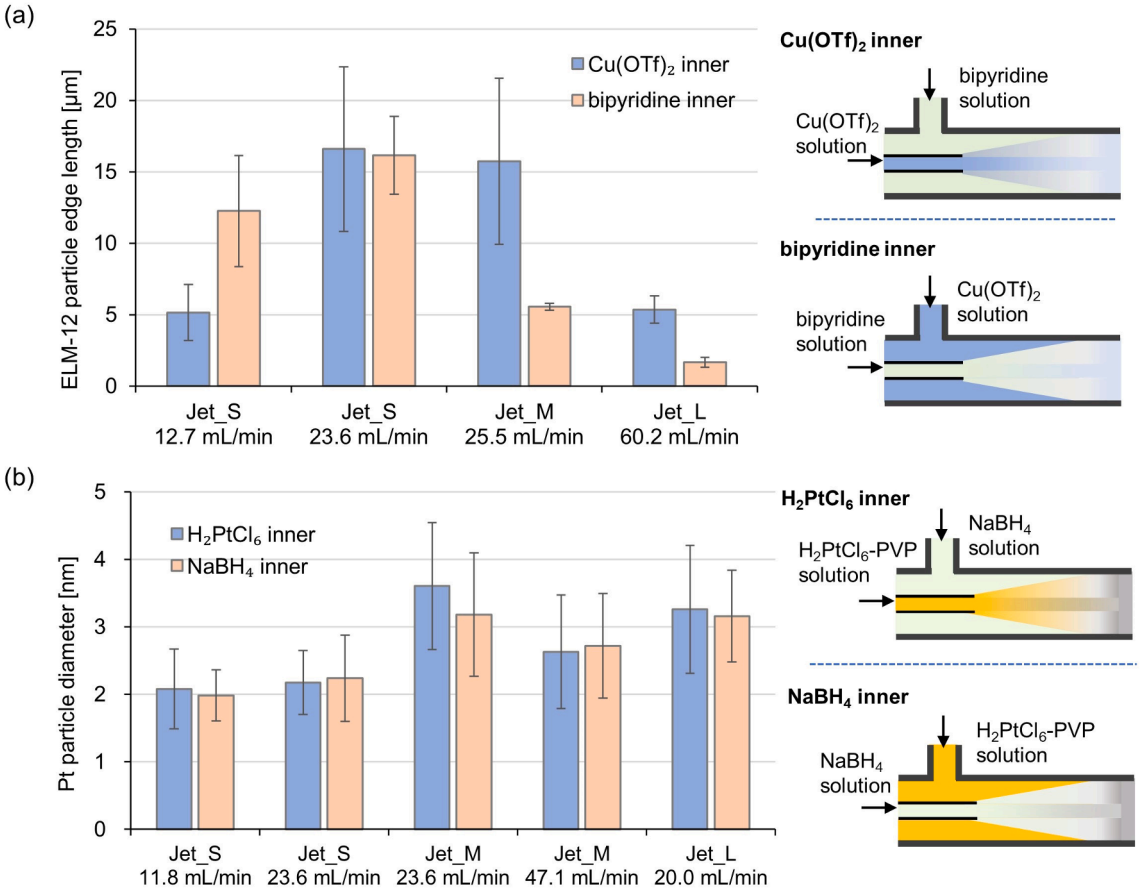

Fig. 7. Size distribution of particles synthesized with microjet mixers: (a) ELM-12 platelets and (b) Pt nanoparticles.

polymorphs can explain the reason. Calcite is the most stable polymorph. Vaterite is the least stable modification of anhydrous $CaCO_3$ [62]. In general, thermodynamically stable polymorph is favored under a nucleation process with small supersaturation. The addition of Na_2CO_3 solution into $CaCl_2$ solution using the batch reactor did not achieve enough supersaturation to form vaterite crystals. Both controlled incorporative mixing profile and the high supersaturation in a microreactor are important for obtaining unstable vaterite crystals selectively.

3.2.2. ELM-12 synthesis

ELM-12 was synthesized using microjet mixers. Diamond-shaped platelets were obtained. Typical SEM images and XRD patterns are provided in Supporting Information. All samples showed peaks at $2\theta =$ 10.0°, 14.0°, 16.5°, 18.0°, 18.5°, and 21.5°, which are consistent with the reported patterns [42,43]. Fig. 7(a) summarizes the size distributions of ELM-12 platelets. The relationship between the particle size and operating conditions with microjet mixers is complicated. The inlet orientation influenced the particle size and its distribution significantly and unpredictably. In the case of Jet_S with a total flow rate of 12.7 mL/min, feeding 4,4′-bipyridine from the inner inlet resulted in more than twice as large particles as those in the other inlet orientations. At a higher flow rate, Jet_S produced larger particles of approximately 16 μm in size, regardless of the inlet orientation. With Jet_M and Jet_L, feeding 4,4′-bipyridine from the inner inlet resulted in smaller particles than with the other orientations.

Unfortunately, it is challenging to give a mechanistic explanation of the relationship between the mixing process and particle sizes in this study. The formation of MOFs is very complex, and their characteristics, like gas adsorption isotherms, can significantly differ by uncertain factors in the synthesis [63]. Incorporative mixing profile and local supersaturation would interact and influence the resulting particle size non-linearly. Although providing a mechanistic explanation is difficult, examination including inlet orientations could achieve the synthesis of monodispersed small particles (1.6 ± 0.35 μm).

3.2.3. Pt nanoparticle synthesis

Fig. 7(b) shows the size distributions of the Pt nanoparticles synthesized in the microjet mixers. In contrast to ELM-12, the inlet orientation had negligible effects on the particle size. Jet_M and Jet_L resulted in larger particle sizes of approximately 3 nm compared with smaller sizes of approximately 2 nm in the Jet_S mixer. The increase in the flow rate with Jet_M also decreased the particle size. Therefore, it can be concluded that faster mixing results in smaller Pt nanoparticles. Notably, only the Pt nanoparticle synthesis was independent of the inlet selection, which had significant influence on the other systems of the Villermaux-Dushman reaction, $CaCO_3$ precipitation, and ELM-12 synthesis.

3.3. Mechanistic insights into the Pt nanoparticle formation

In principle, the effect of mixing originates from the microscopic concentration profile of a microreactor. Therefore, the concentration of the feed solution influences the mixing-sensitivity process. For example, if the acid concentration in the Villermaux-Dushman reaction is doubled, ABS of the outlet solution increases by more than 10 times [26]. Fig. 8 summarizes the sensitivity of the Pt size distribution to the reactant concentrations investigated using the KM-SUS mixer. The variations in the concentration of the reducing agent, [$NaBH_4$], resulted in particle size differences as small as ± 0.09 nm (Fig. 8(a)). In contrast, the concentration of the capping agent, [PVP], was crucial for the particle size (Fig. 8(b)). The decrease in the [PVP]/[Pt^{4+}] ratio from 10 to 5 increased the particle size by 0.27 nm. Further reduction of [PVP]/[Pt^{4+}] to 0.5 obtained large particles with a size of 3.21 nm. Therefore, [PVP], rather than [$NaBH_4$], is crucial for determining the particle size.

Regarding the microscopic mechanism of metal-nanoparticle formation, Polte et al. proposed a model based on the agglomeration of clusters. They reduced $HAuCl_4$ by $NaBH_4$ in a microreactor and characterized the process using an in-line small-angle X-ray scattering setup [64]. They found that the reduction of the precursor was completed within 200 ms, and primary nuclei smaller than 1 nm were formed. Thereafter, the coalescence of the nuclei occurred to form gold nanoparticles with sizes of approximately 2 nm. Yuk et al. confirmed the coalescence of Pt nuclei using in situ TEM analysis [65]. Capping agents, such as PVP, stabilize the facets of the resulting nanoparticles to prevent further agglomeration [66]. Fig. 9 illustrates a plausible model for Pt nanoparticle formation based on that proposed by Polte et al. [64], by modifying it to include the role of PVP. In the 1st stage, the Pt precursor is converted to small nuclei on a sub-nanometer scale through reduction by $NaBH_4$. Although the reduction has very fast kinetics, its reaction rate does not influence the final particle size. The 2nd stage is the coalescence of nuclei to form nanoparticles with diameters of several nanometers. PVP is adsorbed on the facets of the nanoparticles and prevents further attachment of the nuclei. The 2nd step proceeds relatively slowly in the timescale of milliseconds to seconds, but it influences the resulting size of the nanoparticles.

When a local region in a microreactor lacks PVP or is rich in nuclei, the protection of the nanoparticle facets is not sufficient. Therefore, rapid mixing is necessary to produce smaller nanoparticles by uniformly spreading both PVP and nuclei into the entire reactor space. Although the timescale for coalescence is longer than the usual mixing time for microreactors [9,67], the low diffusivity of PVP and nanoclusters renders the mixing time comparable to the coalescence timescale. The diffusion coefficient of Pt nanoparticles is of the order of 10^{-11} m^2 s^{-1} [68]. The diffusion coefficient of PVP is of the same order, considering its molecular weight [69]. They are approximately-one hundredth of the diffusion coefficient of small molecules, including the Pt precursor [68].

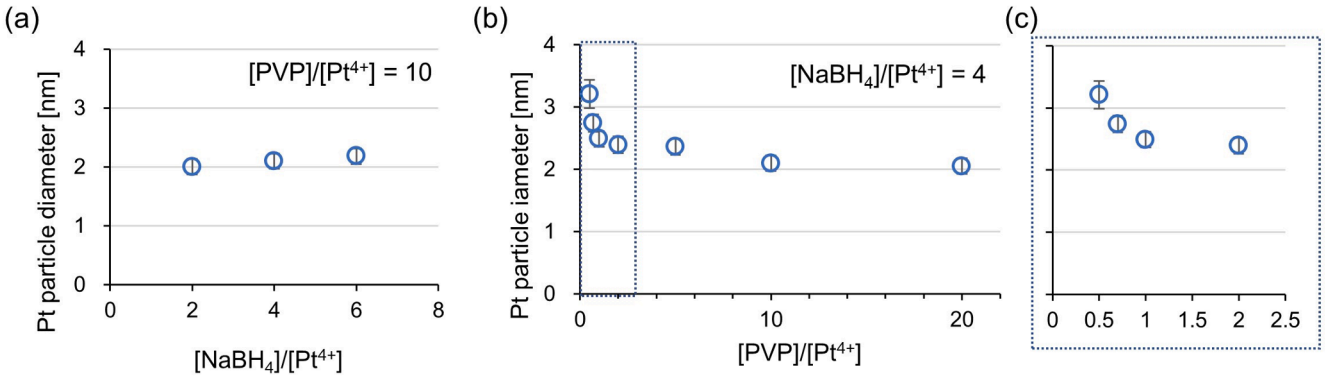

Fig. 8. Effect of the feed concentration on the Pt particle size distribution: (a) reductant concentration and (b, c) capping agent concentration. KM-SUS was employed in all conditions with a total flow rate of 10 mL/min.

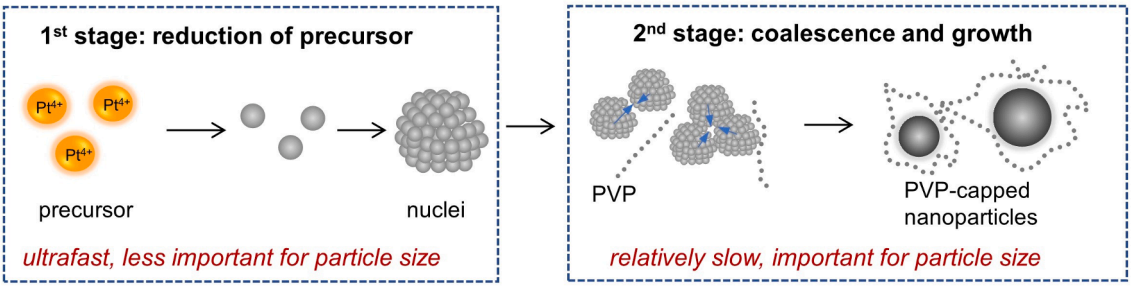

Fig. 9. Supposed mechanism of Pt nanoparticle formation.

Therefore, rapid mixing is important to prevent the agglomeration of Pt nanoclusters but not to promote reactions of the two components. Because the 2nd stage in Fig. 8 consists of physical processes without chemical reactions, the incorporative mixing may not affect the Pt size distribution.

3.4. *Evaluation of mixing profiles based on the size distribution of Pt nanoparticles*

The above findings on Pt nanoparticle synthesis open the possibility of evaluating the physical mixing profile in a microreactor based on the size distribution of the Pt nanoparticles. Fig. 10 presents the size distribution of the Pt nanoparticles obtained using the KM-SUS and tee mixers in a symmetric configuration. The KM-SUS mixer achieved smaller particle sizes than the tee mixer. This is in good agreement with a previous study that demonstrated the better mixing performance of the KM-SUS mixer than tee mixers [40]. In both mixers, a higher flow rate reduced the particle size. This tendency is common to all chemical test reactions [18,19]. We have conducted another set of experiments with changing the outlet tubing length while keeping the flow rate to investigate the effect of residence time. Particle sizes were constant against the tubing length (Figure S8). Thus, the influence of the flow rate on the Pt nanoparticle size is attributed to the mixing effect, not the residence time effect.

Notably, the dispersity of the resulting particle size differed between the KM-SUS and tee mixers. The KM-SUS mixer produced monodispersed nanoparticles, even at a low flow rate of 0.1 mL/min (Fig. 10 (b)). The tee mixer produced small particles similar to the KM-SUS mixer with the highest flow rate of 10 mL/min. However, the standard deviation was 0.21 nm, which is much larger than the value of 0.13 nm obtained with the KM-SUS mixer. According to Fig. 9, the local profile of the PVP concentration and the population density of the clusters would have determined the size distribution of the nanoparticles. The dispersity difference may reflect the uniformity during the mixing process, whereas the average size represents the mixing time.

Fig. 11 shows the tracer concentration profiles of the reactor cross-sections after the confluence, examined using the CFD simulations.

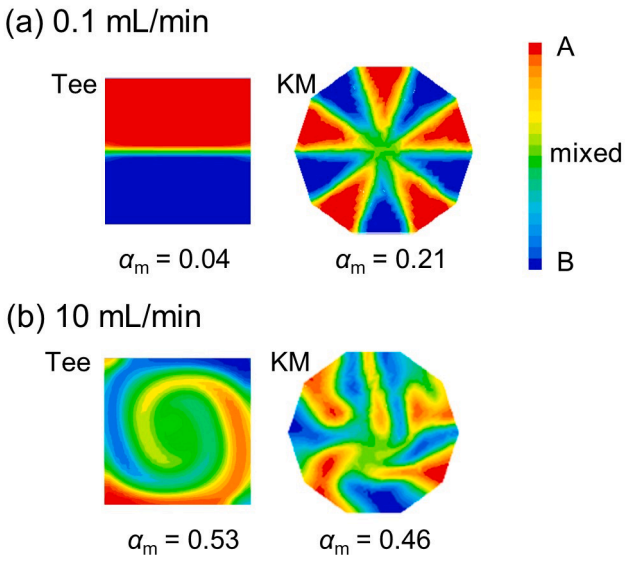

Fig. 11. Contours of the tracer concentration at cross-sections after confluence, obtained through CFD simulations: total flow rate of (a) 0.1 mL/min, and (b) 10 mL/min.

The tee mixier exhibited poor mixing quality at a lower flow rate owing to straight laminar flow [49]. Although laminar flow also formed in the KM mixer at the same flow rate, the pre-divided substreams enabled mixing to proceed via diffusion. At a higher flow rate of 10 mL/min, the vortices in the confluence section promoted mixing through convection. The α_m was slightly higher in the tee mixer. However, the KM mixer exhibited smaller residual segments, whereas the tee mixer had a couple of larger components. These CFD simulations are consistent with the average size and dispersity of the Pt nanoparticles, as shown in Fig. 10 (b). The large dispersity of Pt nanoparticles synthesized in the microjet mixers shown in Fig. 7(b) reflects the nature of unsteady mixing by jetting, wherein a vigorous turbulent stream appears [30].

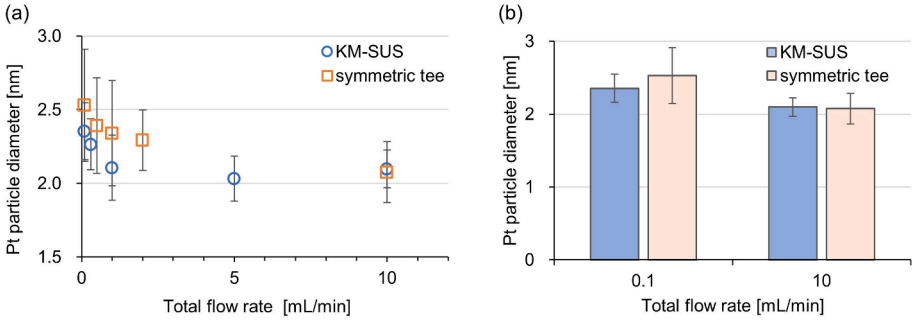

Fig. 10. Pt particle size variation with varying flow rate: (a) entire datasets for the total flow rates of 0.1, 0.3, 0.5, 1.0, 2.0, and 10 mL/min, and (b) selected datasets for mixer comparison.

Based on the above investigation, the use of Pt nanoparticle synthesis as a mixing-evaluation protocol has been proposed. Size distributions of Pt nanoparticles reflect the intensity and uniformity of the mixing process and is independent of the incorporative mixing effect. Unfortunately, size distribution analysis by TEM imaging requires much time and human intervention compared to other chemical test reaction systems. The rapid development of automation technologies in TEM observation and image analysis [70,71] may mitigate these issues in a few years.

4. Conclusions

Experiments and simulations were conducted to confirm the validity of the incorporative mixing model described in Fig. 2, and the following conclusions were drawn:

(1) The incorporative mixing is important not only for competing chemical reactions but also for particle synthesis because the nucleation environment can change by the fluid incorporation.
(2) The inlet orientation of a microreactor is crucial if its two inlets differ in direction, dimension, or position. Two feed streams will undergo different mixing profiles in terms of incorporative mixing. Errors in fabrication can be an unintended source of the difference in the inlet characteristics, resulting in a vast difference in the reaction outcome. Special care regarding the inlet orientation is necessary, except when a microreactor is certified to have identical inlets without fabrication errors.
(3) The incorporative mixing significantly influences the outcome of the chemical test reactions. Therefore, the applicable domain of the test reactions for mixer comparison is much narrower than what is widely assumed. Alternatively, the size distribution of the Pt nanoparticles synthesized by mixing the precursor and reducing agent solutions indicates the physical mixing rate and uniformity.
(4) The consideration of incorporative mixing and optimal inlet orientation will enhance the performance and flexibility of the microreaction technology. It also helps build a model to describe the mixing and reaction mechanisms in microreactors.

Declaration of Competing Interest

The authors declare that they have no known competing financial interests or personal relationships that could have appeared to influence the work reported in this paper.

Data availability

Data will be made available on request.

Acknowledgement

SA and SK acknowledge the support of JSPS KAKENHI (Grant number JP21H05083) and the Cooperative Research Program of Network Joint Research Center for Materials and Devices, which was supported by the Ministry of Education, Culture, Sports, Science, and Technology (MEXT), Japan.

Appendix A. Supplementary data

Supplementary data to this article can be found online at https://doi.org/10.1016/j.cej.2022.138942.

References

[1] A. Hafner, P. Filipponi, L. Piccioni, M. Meisenbach, B. Schenkel, F. Venturoni, J. Sedelmeier, A simple scale-up strategy for organolithium chemistry in flow mode: From feasibility to kilogram quantities, Org. Process Res. Dev. 20 (2016) 1833–1837, https://doi.org/10.1021/acs.oprd.6b00281.
[2] M. Hosoya, S. Nishijima, N. Kurose, Investigation into an unexpected impurity: a practical approach to process development for the addition of grignard reagents to aldehydes using continuous flow synthesis, Org. Process Res. Dev. 24 (2020) 405–414, https://doi.org/10.1021/acs.oprd.9b00515.
[3] T. Sato, New synthetic method of nanoparticles by micro chemical process technology, Fujifilm Res. Dev. Jpn. 53 (2008) 21–26.
[4] J.I. Yoshida, Y. Takahashi, A. Nagaki, Flash chemistry: Flow chemistry that cannot be done in batch, Chem. Commun. 49 (2013) 9896–9904, https://doi.org/10.1039/c3cc44709j.
[5] H. Shi, K. Nie, B. Dong, L. Chao, F. Gao, M. Ma, M. Long, Z. Liu, Mixing enhancement via a serpentine micromixer for real-time activation of carboxyl, Chem. Eng. J. 392 (2020), 123642, https://doi.org/10.1016/j.cej.2019.123642.
[6] R. Okabe, N. Sugisawa, S. Fuse, A micro-flow rapid dual activation approach for urethane-protected α-amino acid *N* -carboxyanhydride synthesis, Org. Biomol. Chem. 20 (16) (2022) 3303–3310.
[7] N. Sugisawa, H. Sugisawa, Y. Otake, R.V. Krems, H. Nakamura, S. Fuse, Rapid and mild one-flow synthetic approach to unsymmetrical sulfamides guided by bayesian optimization, Chemistry-Methods. 1 (2021) 484–490, https://doi.org/10.1002/cmtd.202100053.
[8] H. Kim, A. Nagaki, J.I. Yoshida, A flow-microreactor approach to protecting-group-free synthesis using organolithium compounds, Nat. Commun. 2 (2011) 264–266, https://doi.org/10.1038/ncomms1264.
[9] S. Asano, S. Yatabe, T. Maki, K. Mae, Numerical and experimental quantification of the performance of microreactors for scaling-up fast chemical reactions, Org. Process Res. Dev. 23 (2019) 807–817, https://doi.org/10.1021/acs.oprd.8b00356.
[10] D. Yamamoto, T. Maki, S. Watanabe, H. Tanaka, M.T. Miyahara, K. Mae, Synthesis and adsorption properties of ZIF-8 nanoparticles using a micromixer, Chem. Eng. J. 227 (2013) 145–150, https://doi.org/10.1016/j.cej.2012.08.065.
[11] J. Han, Z. Zhu, H. Qian, A.R. Wohl, C.J. Beaman, T.R. Hoye, C.W. Macosko, A simple confined impingement jets mixer for flash nanoprecipitation, J. Pharm. Sci. 101 (2012) 4018–4023, https://doi.org/10.1002/jps.23259.
[12] K. Inohara, S. Asano, T. Maki, K. Mae, Synthesis of small lipid nanoparticles using an inkjet mixing system aiming to reduce drug loss, Chem. Eng. Technol. 42 (2019) 2061–2066, https://doi.org/10.1002/ceat.201900041.
[13] S. Watanabe, T. Koshiyama, T. Watanabe, M.T. Miyahara, Room-temperature synthesis of Ni and Pt-Co Alloy nanoparticles using a microreactor, Front. Chem. Eng. 3 (2021), 780384, https://doi.org/10.3389/fceng.2021.780384.
[14] Y. Gao, B. Pinho, L. Torrente-Murciano, Tailoring the size of silver nanoparticles by controlling mixing in microreactors, Chem. Eng. J. 432 (2022), 134112, https://doi.org/10.1016/j.cej.2021.134112.
[15] (n.d.). https://doi.org/10.1016/j.cej.2021.128565.
[16] S. Tomasi Masoni, M. Antognoli, A. Mariotti, R. Mauri, M.V. Salvetti, C. Galletti, E. Brunazzi, Flow regimes, mixing and reaction yield of a mixture in an X-microreactor, Chem. Eng. J. 437 (2022), 135113, https://doi.org/10.1016/j.cej.2022.135113.
[17] J.M. Reckamp, A. Bindels, S. Duffield, Y.C. Liu, E. Bradford, E. Ricci, F. Susanne, A. Rutter, Mixing performance evaluation for commercially available micromixers using villermaux-dushman reaction scheme with the interaction by exchange with the mean model, Org. Process Res. Dev. 21 (2017) 816–820, https://doi.org/10.1021/acs.oprd.6b00332.
[18] S. Schwolow, J. Hollmann, B. Schenkel, T. Röder, Application-oriented analysis of mixing performance in microreactors, Org. Process Res. Dev. 16 (2012) 1513–1522, https://doi.org/10.1021/op300107z.
[19] K.J. Hecht, A. Kölbl, M. Kraut, K. Schubert, Micromixer characterization with competitive-consecutive bromination of 1,3,5-trimethoxybenzene, Chem. Eng. Technol. 31 (2008) 1176–1181, https://doi.org/10.1002/ceat.200800213.
[20] J.R. Bourne, O.M. Kut, J. Lenzner, H. Maire, Kinetics of the Diazo Coupling between 1-Naphthol and Diazotized Sulfanilic Acid, Ind. Eng. Chem. Res. 29 (1990) 1761–1765, https://doi.org/10.1021/ie00105a004.
[21] J.R. Bourne, F. Kozicki, Mixing effects during the bromination of 1,3,5-trimethoxybenzene, Chem. Eng. Sci. 32 (1977) 1538–1539, https://doi.org/10.1016/0009-2509(77)80255-8.
[22] Y. Endo, M. Furusawa, T. Shimazaki, Y. Takahashi, Y. Nakahara, A. Nagaki, Molecular weight distribution of polymers produced by anionic polymerization enables mixability evaluation, Org. Process Res. Dev. 23 (2019) 635–640, https://doi.org/10.1021/acs.oprd.8b00403.
[23] A.P. LaGrow, M.O. Besenhard, A. Hodzic, A. Sergides, L.K. Bogart, A. Gavriilidis, N. T.K. Thanh, Unravelling the growth mechanism of the co-precipitation of iron oxide nanoparticles with the aid of synchrotron X-Ray diffraction in solution, Nanoscale. 11 (2019) 6620–6628, https://doi.org/10.1039/C9NR00531E.
[24] A.N. Manzano Martínez, A. Chaudhuri, M. Assirelli, J. van der Schaaf, Effects of increased viscosity on micromixing in rotor–stator spinning disk reactors, Chem. Eng. J. 434 (2022), 134292, https://doi.org/10.1016/j.cej.2021.134292.
[25] M.C. Fournier, L. Falk, J. Villermaux, A new parallel competing reaction system for assessing micromixing efficiency - Experimental approach, Chem. Eng. Sci. 51 (1996) 5053–5064, https://doi.org/10.1016/0009-2509(96)00270-9.
[26] J.M. Commenge, L. Falk, Villermaux-Dushman protocol for experimental characterization of micromixers, Chem. Eng. Process. Process Intensif. 50 (2011) 979–990, https://doi.org/10.1016/j.cep.2011.06.006.
[27] E. Arian, W. Pauer, Contributions to the kinetics of the iodide–iodate test reaction for micromixing time calculation with extended incorporation models, Chem. Eng. Sci. 237 (2021), 116549, https://doi.org/10.1016/j.ces.2021.116549.
[28] N. Di Patrizio, M. Bagnaro, A. Gaunand, J.F. Hochepied, D. Horbez, P. Pitiot, Hydrodynamics and mixing performance of Hartridge Roughton mixers: Influence

of the mixing chamber design, Chem. Eng. J. 283 (2016) 375–387, https://doi.org/10.1016/j.cej.2015.06.116.
[29] A. Kölbl, M. Kraut, On the use of the Iodide Iodate Reaction Method for assessing mixing times in continuous flow mixers, AIChE J. 57 (2011) 835–840, https://doi.org/10.1002/aic.12313.
[30] S. Asano, S. Yamada, T. Maki, Y. Muranaka, K. Mae, Design protocol of microjet mixers for achieving desirable mixing times with arbitrary flow rate ratios, React, Chem. Eng. 2 (2017) 830–841, https://doi.org/10.1039/C7RE00051K.
[31] J. Baldyga, J.R. Bourne, Simplification of micromixing calculations. I. Derivation and application of new model, Chem. Eng. J. 42 (1989) 83–92, https://doi.org/10.1016/0300-9467(89)85002-6.
[32] J. Baldyga, J.R. Bourne, Simplification of micromixing calculations. II. New applications, Chem. Eng. J. 42 (1989) 93–101, https://doi.org/10.1016/0300-9467(89)85003-8.
[33] R. Lebl, D. Cantillo, C.O. Kappe, Continuous generation, in-line quantification and utilization of nitrosyl chloride in photonitrosation reactions, React, Chem. Eng. 4 (2019) 738–746, https://doi.org/10.1039/C8RE00323H.
[34] M.A. Morin, W. Zhang, D. Mallik, M.G. Organ, Sampling and Analysis in Flow: The Keys to Smarter, More Controllable, and Sustainable Fine-Chemical Manufacturing, Angew. Chem. - Int. Ed. 60 (2021) 20606–20626, https://doi.org/10.1002/ANIE.202102009.
[35] T. Fukuyama, M. Kobayashi, M.T. Rahman, N. Kamata, I. Ryu, Spurring radical reactions of organic halides with tin hydride and TTMSS using microreactors, Org. Lett. 10 (2008) 533–536, https://doi.org/10.1021/ol702718z.
[36] M.B. Plutschack, B. Pieber, K. Gilmore, P.H. Seeberger, The hitchhiker's guide to flow chemistry, Chem. Rev. 117 (2017) 11796–11893, https://doi.org/10.1021/acs.chemrev.7b00183.
[37] H. Cheng, B. Huang, Y. Dai, X. Qin, X. Zhang, One-step synthesis of the nanostructured AgI/BiOI composites with highly enhanced visible-light photocatalytic performances, Langmuir 26 (2010) 6618–6624, https://doi.org/10.1021/la903943s.
[38] A.R. Abbasi, A. Morsali, Syntheses and characterization of AgI nano-structures by ultrasonic method: Different morphologies under different conditions, Ultrason. Sonochem. 17 (2010) 572–578, https://doi.org/10.1016/j.ultsonch.2009.11.002.
[39] H. Li, H. Xia, D. Wang, X. Tao, Simple synthesis of monodisperse, quasi-spherical, citrate-stabilized silver nanocrystals in water, Langmuir 29 (2013) 5074–5079, https://doi.org/10.1021/la400214x.
[40] H. Nagasawa, N. Aoki, K. Mae, Design of a new micromixer for instant mixing based on the collision of micro segments, Chem. Eng. Technol. 28 (2005) 324–330, https://doi.org/10.1002/ceat.200407118.
[41] S. Asano, T. Maki, K. Mae, Evaluation of mixing profiles for a new micromixer design strategy, AIChE J. 62 (2016) 1154–1161, https://doi.org/10.1002/aic.15082.
[42] A. Kondo, H. Noguchi, L. Carlucci, D.M. Proserpio, G. Ciani, H. Kajiro, T. Ohba, H. Kanoh, K. Kaneko, Double−step gas sorption of a two−dimensional metal−organic framework, J. Am. Chem. Soc. 129 (2007) 12362–12363, https://doi.org/10.1021/ja073568h.
[43] F.J. Sotomayor, C.M. Lastoskie, Carbon dioxide capacity retention on elastic layered metal organic frameworks subjected to hydrothermal cycling, Microporous Mesoporous Mater. 304 (2020), 110377, https://doi.org/10.1016/j.micromeso.2020.110377.
[44] S. Watanabe, S. Hiraide, H. Kunimitsu, A. Fujiwara, M.T. Miyahara, Mechanism of CO2 Capacity Reduction of Flexible Metal-Organic Framework Caused by Water Adsorption, Front. Mater. 9 (2022), 825592, https://doi.org/10.3389/fmats.2022.825592.
[45] R.B. Bird, W.E. Stewart, E.N. Lightfoot, Transport Phenomena, John Wiley & Sons Inc, 2006.
[46] S. Hardt, F. Schönfeld, Laminar mixing in different interdigital micromixers: II, Numerical simulations, AIChE J. 49 (2003) 578–584, https://doi.org/10.1002/aic.690490305.
[47] D.M. Roberge, L. Ducry, N. Bieler, P. Cretton, B. Zimmermann, Microreactor technology: A revolution for the fine chemical and pharmaceutical industries? Chem. Eng. Technol. 28 (2005) 318–323, https://doi.org/10.1002/ceat.200407128.
[48] A. Nagaki, S. Ishiuchi, K. Imai, K. Sasatsuki, Y. Nakahara, J.I. Yoshida, Micromixing enables chemoselective reactions of difunctional electrophiles with functional aryllithiums, React, Chem. Eng. 2 (2017) 862–870, https://doi.org/10.1039/c7re00142h.
[49] S. Dreher, N. Kockmann, P. Woias, Characterization of laminar transient flow regimes and mixing in t-shaped micromixers, Heat Transf. Eng. 30 (2009) 91–100, https://doi.org/10.1080/01457630802293480.
[50] N. Aoki, T. Fukuda, N. Maeda, K. Mae, Design of confluence and bend geometry for rapid mixing in microchannels, Chem. Eng. J. 227 (2013) 198–202, https://doi.org/10.1016/j.cej.2012.03.061.
[51] M. Rahimi, P. Valeh-e-Sheyda, M.A. Parsamoghadam, N. Azimi, H. Abidi, LASP and Villermaux/Dushman protocols for mixing performance in microchannels: Effect of geometry on micromixing characterization and size reduction, Chem. Eng. Process. Process Intensif. 85 (2014) 178–186, https://doi.org/10.1016/j.cep.2014.09.001.
[52] U. Fatima, M. Shakaib, I. Memon, Analysis of mass transfer performance of micromixer device with varying confluence angle using CFD, Chem. Pap. 74 (2020) 1267–1279, https://doi.org/10.1007/s11696-019-00975-8.
[53] M. Garcia-Cardosa, F.-J. Granados-Ortiz, J. Ortega-Casanova, A Review on Additive Manufacturing of Micromixing Devices, Micromachines. 13 (2021) 73, https://doi.org/10.3390/mi13010073.
[54] D. Koo, H. So, Facile microfabrication of three dimensional-patterned micromixers using additive manufacturing technology, Sci. Rep. 12 (2022) 6346, https://doi.org/10.1038/s41598-022-10356-z.
[55] Y. Murakami, A. Shono, Reaction engineering with recurrent neural network: Kinetic study of Dushman reaction, Chem. Eng. J. Adv. 9 (2022), 100219, https://doi.org/10.1016/j.ceja.2021.100219.
[56] N. Rajabi, M. Hoffmann, J. Bahnemann, A.P. Zeng, M. Schlüter, J. Müller, A chaotic advection enhanced microfluidic split-and-recombine mixer for the preparation of chemical and biological probes, J. Chem. Eng. Jpn. 45 (2012) 703–707, https://doi.org/10.1252/jcej.12we071.
[57] N. Kockmann, T. Kiefer, M. Engler, P. Woias, Convective mixing and chemical reactions in microchannels with high flow rates, Sens. Actuators B Chem. 117 (2006) 495–508, https://doi.org/10.1016/j.snb.2006.01.004.
[58] C. Galletti, M. Roudgar, E. Brunazzi, R. Mauri, Effect of inlet conditions on the engulfment pattern in a T-shaped micro-mixer, Chem. Eng. J. 185–186 (2012) 300–313, https://doi.org/10.1016/j.cej.2012.01.046.
[59] S. Choi, R. Karnik, R. Langer, J.-M. Lim, O.C. Farokhzad, A. Swami, J. Wu, S. Chopra, L.M. Gilson, Ultra-high throughput synthesis of nanoparticles with homogeneous size distribution using a coaxial turbulent jet mixer, ACS Nano 8 (2014) 6056–6065, https://doi.org/10.1021/nn501371n.
[60] J.H.E. Cartwright, A.G. Checa, J.D. Gale, D. Gebauer, C.I. Sainz-Díaz, Calcium carbonate polyamorphism and its role in biomineralization: How many amorphous calcium carbonates are there? Angew. Chem. - Int. Ed. 51 (2012) 11960–11970, https://doi.org/10.1002/anie.201203125.
[61] M. Kogo, T. Umegaki, Y. Kojima, Effect of pH on formation of single-phase vaterite, J. Cryst. Growth. 517 (2019) 35–38, https://doi.org/10.1016/j.jcrysgro.2019.04.005.
[62] A.S. Schenk, E.J. Albarracin, Y.Y. Kim, J. Ihli, F.C. Meldrum, Confinement stabilises single crystal vaterite rods, Chem. Commun. 50 (2014) 4729–4732, https://doi.org/10.1039/c4cc01093k.
[63] J. Park, J.D. Howe, D.S. Sholl, How reproducible are isotherm measurements in metal-organic frameworks? Chem. Mater. 29 (2017) 10487–10495, https://doi.org/10.1021/acs.chemmater.7b04287.
[64] J. Polte, R. Erler, A.F. Thünemann, S. Sokolov, T.T. Ahner, K. Rademann, F. Emmerling, R. Kraehnert, Nucleation and growth of gold nanoparticles studied *via in situ* small angle X-ray scattering at millisecond time resolution, ACS Nano 4 (2010) 1076–1082, https://doi.org/10.1021/nn901499c.
[65] J.M. Yuk, J. Park, P. Ercius, K. Kim, D.J. Hellebusch, M.F. Crommie, J.Y. Lee, A. Zettl, A.P. Alivisatos, High-resolution EM of colloidal nanocrystal growth using graphene liquid cells, Science 335 (2012) 61–64, https://doi.org/10.1126/science.1217654.
[66] Y. Xia, Y. Xiong, B. Lim, S.E. Skrabalak, Shape-controlled synthesis of metal nanocrystals: Simple chemistry meets complex physics? Angew. Chem. - Int. Ed. 48 (2009) 60–103, https://doi.org/10.1002/anie.200802248.
[67] H. Kim, K.I. Min, K. Inoue, D.J. Im, D.P. Kim, J.I. Yoshida, Submillisecond organic synthesis: Outpacing Fries rearrangement through microfluidic rapid mixing, Science 352 (2016) 691–694, https://doi.org/10.1126/science.aaf1389.
[68] M. Harada, K. Okamoto, M. Terazima, Diffusion of platinum ions and platinum nanoparticles during photoreduction processes using the transient grating method, Langmuir 22 (2006) 9142–9149, https://doi.org/10.1021/la061663i.
[69] M.G. Davidson, W.M. Deen, Hindered diffusion of water-soluble macromolecules in membranes, Macromolecules 21 (1988) 3474–3481, https://doi.org/10.1021/ma00190a022.
[70] H. Tan, W. Weng, R. Rai, C. Kang, L. Dumas, I. Brooks, A. Katnani, Z. Zhong, C. Hakala, Y. Lu, J. Fretwell, T.A. Johnson, Advanced industrial S, TEM automation and metrology: Boundary of precision, in, 29th Annu. SEMI Adv. Semicond. Manuf. Conf ASMC, IEEE, Saratoga Springs, NY, USA 2018 (2018) 131–135, https://doi.org/10.1109/ASMC.2018.8373156.
[71] A. Colliard-Granero, M. Batool, J. Jankovic, J. Jitsev, M.H. Eikerling, K. Malek, M. J. Eslamibidgoli, Deep learning for the automation of particle analysis in catalyst layers for polymer electrolyte fuel cells, Nanoscale. 14 (2022) 10–18, https://doi.org/10.1039/D1NR06435E.